Science Arts & Métiers (SAM)
is an open access repository that collects the work of Arts et Métiers Institute of Technology researchers and makes it freely available over the web where possible.

This is an author-deposited version published in: https://sam.ensam.eu
Handle ID: .http://hdl.handle.net/10985/21439

To cite this version :

Catherine WEISMAN, Diana BALTEAN-CARLÈS, Hélène BAILLIET, Virginie DARU - A numerical study of the coupling between Rayleigh streaming and heat transfer at high acoustic level - The Journal of the Acoustical Society of America - Vol. 150, n°6, p.4501-4510 - 2021

Any correspondence concerning this service should be sent to the repository Administrator : scienceouverte@ensam.eu

A numerical study of the coupling between Rayleigh streaming and heat transfer at high acoustic level

Virginie Daru,[1] Catherine Weisman,[2] Diana Baltean-Carlès,[2] and Hélène Bailliet[3]
[1] *DynFluid Lab., ENSAM, 151 Boulevard de l'Hôpital, 75013, Paris, France & LISN, CNRS, Université Paris-Saclay, Bât. 507, Rue John Von Neumann, Campus Universitaire, F-91405 Orsay Cedex, France*
[2] *Sorbonne Université, CNRS, Institut Jean Le Rond d'Alembert, ∂'Alembert, 4 Place Jussieu, 75005 Paris, France*
[3] *Institut Pprime, CNRS - Université de Poitiers - ENSMA, ENSIP, 6 rue Marcel Doré, Bât. B17 - BP 633, 86022 Poitiers Cedex, France*[a]

Complex coupling between thermal effects and Rayleigh streaming in a standing wave guide at high acoustic levels is analyzed numerically. The approach is guided by our recent analytical study showing that reverse streaming cells can form if the nonlinear Reynolds number exceeds a value depending on the wave frequency and on thermophysical properties of the fluid and solid wall. A numerical configuration is introduced to investigate the evolution of the streaming flow structure and average temperature field at high acoustic levels. Special attention is given to inhibit the development of shock waves. Heat conduction is accounted for in the wall. As the acoustic level is increased, the average temperature field becomes stratified transversely. Simulations show the relevance of the criterion for characterizing the appearance of new contra-rotating streaming cells near the acoustic velocity antinodes. For higher acoustic levels these new cells evolve into increasingly large stagnant zones where the streaming flow is of very small amplitude and contours of temperature are stratified longitudinally. The overall outer streaming flow decreases. These results are consistent with previous experimental observations showing that the intrinsic coupling between thermal effects and acoustic streaming at high levels is very well described.

https://doi.org/10.1121/10.0009026

I. INTRODUCTION

Rayleigh streaming[1] usually refers to acoustic streaming generated in a cylindrical standing wave guide by Reynolds stresses in the Stokes boundary layer of the oscillating fluid near the solid wall. It is a second order phenomenon superimposed to the first order acoustic oscillation. Acoustic streaming is important in particular in the field of thermoacoustics because it is associated with heat convection in thermoacoustic engines or refrigerators and can reduce their efficiency[2]. Working conditions for these devices are generally associated with high intensity waves and the behavior of acoustic streaming in this case has been the subject of numerous experimental and numerical studies over the last 20 years.

At low acoustic amplitudes, the Rayleigh streaming flow is composed of so-called "inner" and "outer" toroidal vortices that have a half-wavelength spatial periodicity. They are well described by Rayleigh-Nyborg-Westervelt (RNW)

[a] helene.bailliet@univ-poitiers.fr

streaming theory[3], valid for low acoustic amplitudes, also called "slow regime".

For high acoustic levels, in the so-called "fast regime", it was found both experimentally[4,5,6] and numerically[7,8,9] that as the acoustic level is increased, the streaming pattern for the outer vortices is modified and additional counter rotating vortices may appear in the center of the guide near the acoustic velocity antinodes. This behavior was found to be followed by outer streaming cells only, the inner streaming vortices being slightly modified by high acoustic levels.

The nonlinear Reynolds number Re_{NL} is commonly used in the literature to separate the two regimes: $Re_{NL} \ll 1$ for slow streaming and $Re_{NL} > 1$ for fast streaming[10]. It is defined as $Re_{NL} = (M \times R/\delta_\nu)^2$, where M is the acoustic Mach number, $M = U_{ac}/c_0$, with U_{ac} the maximum acoustic velocity amplitude on the axis and c_0 the initial speed of sound, R being the radius of the guide and $\delta_\nu = \sqrt{2\nu/\omega}$ the viscous boundary layer thickness, ν being the kinematic viscosity and ω the wave angular frequency. Re_{NL} can be viewed as the Reynolds number of the outer streaming flow.

In the last decade our team has worked on this distortion of the streaming flow in the fast regime. A first joint experimental and numerical study (based on the fully compressible Navier-Stokes equations) of the evolution of Rayleigh streaming was performed[11] from slow to fast regime. It was found that the experimental and numerical streaming patterns evolved in a similar manner and that new counter-rotating vortices appeared near the velocity acoustic antinodes for a similar value of the nonlinear Reynolds number.

We then attempted to analyze separately each phenomenon that could explain this evolution at high acoustic amplitudes: inertia, non linear coupling between acoustics and streaming, thermal effects, nonlinear acoustic propagation. Our first focus was on analyzing the effect of inertia, controlled by Re_{NL}. Thermal effects were suppressed in numerical simulations by considering isentropic waves. Also, shock waves being known for generating entropy, their effect was expected to be small in these isentropic simulations[9,12]. A similar evolution of the streaming flow as in[11] was observed but at higher Re_{NL}[9]. These results highlighted the main role of non linear coupling between acoustic and streaming flows[12], and showed that inertia affected the streaming flow only slightly (in accordance with the theoretical results of[10]). More recently our focus turned to thermal effects.

The crucial role of temperature effects on Rayleigh streaming was pointed out by Thompson and Atchley[4]. They found a strong correlation between an axial mean temperature gradient on the wall guide and the axial streaming velocity, although a clear explanation of the physical reason could not be provided at this stage: "The observed steady-state streaming velocities are not in agreement with any available theory".

In more recent numerical[13,14] and theoretical studies[15,16] it was shown that a transverse mean temperature gradient has a huge impact: Červenka and Bednařík[13,14] showed that a temperature difference of a few degrees only over the resonator's section is sufficient to reverse the outer Rayleigh streaming flow. In[16], an analytical study was conducted exhibiting the important role of a conducting thick wall in inducing an axial temperature gradient in the fluid through combined thermoacoustic effect and conduction in the wall. This in turn generates a transverse mean temperature gradient through convective transport by the streaming flow[14]. In the end, appropriate scaling parameters for describing acoustic streaming at high acoustic levels were found: The streaming flow is strongly modified and a reverse flow is obtained if the nonlinear Reynolds number Re_{NL} exceeds a parameter denoted K_c, which depends on the thermo-physical characteristics of the fluid and the wall, and on the wave frequency.

In light of these recent results that reveal the importance of thermal effects in general and of thermal stratification in particular, a numerical study of Rayleigh streaming at high acoustic levels is proposed in the present paper. Special attention is given to inhibit the development of shock waves, since they have important effects on the thermal field[17]. In our previous numerical simulations of the complete Navier-Stokes equations[8] large temperature variations were observed, probably due to the presence of shock waves. In numerical simulations of acoustic streaming developing within a solely straight tube, shock waves were shown to be present as soon as the acoustic amplitude exceeds a relatively low level[18,19], with the exception of[7] that used specific boundary conditions (acous-

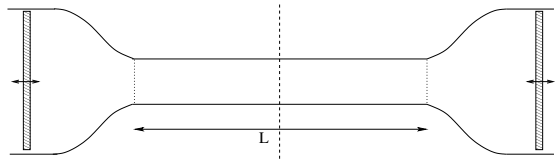

FIG. 1. Sketch of the geometry.

tic wave created by two in-phase sources). On the contrary, there is no shock wave in our reference experiments[6,11]. Thus we here consider a tube with varying cross section that mimics the experimental apparatus and creates a quasi mono-frequency wave. To our knowledge, this is the first numerical simulation at high acoustic levels without any shock wave. Also since the role of a conducting wall was shown to be important[7,20], the wall thickness is taken into account and the heat equation is solved inside the wall, which is also a novelty of the present study. The new criterion found analytically[16] is shown to be adequate. This yields much better comparison with experimental results than those obtained previously and therefore is a step forward in understanding the evolution of streaming at high acoustic levels. This approach helps disentangling the effects of different phenomena on acoustic streaming: non linear propagation, acoustically-driven convection in the fluid, boundary conditions.

In Section II, we present the cases under study and the numerical configurations, as well as physical and numerical parameters. We then present in Section III the numerical results obtained for low acoustic amplitude. The acoustic, mean temperature and velocity fields are analyzed. Section IV is dedicated to high acoustic amplitudes. A first simulation is performed with a surrounding wall of zero-thickness (ideal isothermal boundary condition), illustrating the effect of reducing the harmonic content of the acoustic wave. Then in the case of a thick conducting wall two values of the guide's radius and of the wall thickness are considered in order to assess the adequacy of the parameter K_C in predicting the evolution of the streaming field[16]. The time evolution of the fields are analyzed.

II. PROBLEM DESCRIPTION AND NUMERICAL MODEL.

A. Numerical configuration

The object of this study is the streaming field inside a cylindrical straight tube filled with fluid submitted to a mono-frequency acoustic wave. As stated in the introduction, we consider here a numerical configuration specifically designed to reduce the harmonic content of the acoustic wave and avoid the appearance of shock waves. This geometry (Fig.1) is analogous to that reported in experiments[6]. In these experiments, the acoustic wave is created by two loudspeakers placed at each extremity of the wave guide. Two convergent tubes connect each loudspeaker to the straight middle part of the guide, in order to reduce sharp section changes. It follows that the harmonic acoustic cascade is inhibited, and the acoustic wave is nearly mono-frequency. The central straight tube is cylindrical of length L and radius R. In the calculation, two oscillating pistons are placed at the extremities of the guide and create the acoustic wave. They are modeled as moving cylinders of radius greater than R. Two converging tubes of length $L/4$ each connect the piston and the middle straight tube.

The guide is initially filled with the working gas. Since the pistons are operated in opposite phase, the problem is antisymmetric with respect to a vertical axis that passes through the center of the tube (vertical dashed line in Fig. 1). In the following, we will thus only consider the right half of the configuration (the half length of the tube connected to one piston). The working acoustic frequency, noted f, is the third resonant frequency of the straight tube, so that the wavelength $\lambda = c_0/f$ satisfies $L = 3\lambda/2$. Therefore we expect the formation of 6 acoustic streaming cells along the entire straight portion of the tube, three of which falling within the simulation configuration. The two central streaming cells are not much affected by side effects due to the vicinity of the converging section.

The flow is considered to be axisymmetric, modeled by the fully compressible Navier-Stokes

equations:

$$\begin{cases} \frac{\partial \rho}{\partial t} + \nabla \cdot (\rho \mathbf{v}) = 0 \\ \frac{\partial (\rho \mathbf{v})}{\partial t} + \nabla \cdot (\rho \mathbf{v} \otimes \mathbf{v}) + \nabla p = \nabla \cdot \bar{\bar{\tau}} \\ \frac{\partial (\rho E)}{\partial t} + \nabla \cdot (\rho E \mathbf{v} + p \mathbf{v}) = \nabla \cdot (k \nabla T + \bar{\bar{\tau}} \mathbf{v}) \end{cases} \quad (1)$$

where $\mathbf{v} = (u, v)^T$ is the flow velocity, $E = e + \frac{1}{2}\mathbf{v} \cdot \mathbf{v}$ is the total energy, with $e = \frac{p}{(\gamma-1)\rho}$ the internal energy, p the pressure, ρ the density, γ the specific heat ratio, $\bar{\bar{\tau}} = -\frac{2}{3}\mu(\nabla \cdot \mathbf{v})\bar{\bar{I}} + 2\mu\bar{\bar{D}}$ the viscous stress tensor of a Newtonian fluid, $\bar{\bar{I}}$ being the identity tensor, $\bar{\bar{D}} = \frac{1}{2}(\nabla \mathbf{v} + \nabla^T \mathbf{v})$ the strain tensor, μ the dynamic viscosity, k the thermal conductivity. The gas is considered as a perfect gas obeying the state law $p = r_g \rho T$, where T is the temperature and r_g is the perfect gas constant.

Boundary conditions for velocity are: no slip on walls and symmetry on the axis and on the left end of the simulation domain. The piston and wall of the convergent tube are set isothermal at ambient temperature T_0. The straight part of the tube is surrounded by a conducting wall, within which the heat equation is solved. The wall, of thickness w, is made of a solid material of thermal conductivity k_s, density ρ_s and specific heat c_s. The surrounding gas is considered as a thermostat at ambient temperature (wall-air convection is neglected and the outside wall temperature is set equal to the ambient temperature). A zero radial temperature gradient is imposed on the symmetry axis. Boundary conditions on the convergent tube wall are treated in the fixed grid using an immersed boundary approach[21]. An Arbitrary Lagrangian-Eulerian method[22] (ALE) is applied to the grid portion surrounding the piston in order to impose the piston movement, the corresponding grid portion being moving and deformable.

The model is solved numerically by using high order finite difference schemes, developed in[23]. An upwind scheme, third order accurate in time and space, is used for convective terms, and a centered scheme, second order, is used for diffusion terms. The numerical scheme being explicit, the time step δt is fixed such as to satisfy the stability condition: $\delta t \leq \frac{1}{2}\delta r / c_0$, with δr the minimum cell size in the radial direction. Finally, any fluid variable ϕ is separated, using Reynolds decomposition, into a fluctuating, periodic, component ϕ', and its mean value $\overline{\phi}$ according to $\phi = \overline{\phi} + \phi'$. The mean flow is obtained from calculating a simple mean value for each physical quantity (velocity, density, pressure, temperature) over an acoustic period. Concerning the streaming velocity, the average mass transport velocity $\overline{\mathbf{v}}^M = \overline{\mathbf{v}} + \frac{\overline{\rho' \mathbf{v}'}}{\overline{\rho}}$ ($\overline{\mathbf{v}}$ being the Eulerian streaming velocity) will be shown in the following, since it is responsible for the convective heat transport.

B. Physical and numerical parameters

In all simulations presented thereafter, the tube is initially filled with air at standard thermodynamic conditions, $p_0 = 101325$ Pa, $\rho_0 = 1.2$ kg.m^{-3}, $T_0 = 294.15$ K. The thermo-physical properties of air are $\mu = 1.795\ 10^{-5}$ kg.m^{-1}s^{-1} and $k = 0.025$ W.m^{-1}.K^{-1}. Also for air, $\gamma = 1.4$ and $r_g = 287.06$ J.kg^{-1}.K^{-1}. This results in an initial speed of sound $c_0 = 343.82$ m.s^{-1}. The Prandtl number Pr is equal to 0.726. Having taken into consideration numerical constraints, the central length of the tube is fixed $L = 0.026$ m. This corresponds to a wave of frequency $f = 20000$ Hz. The resulting boundary layer thickness is $\delta_\nu = 1.54\ 10^{-5}$ m. The dimensions of the numerical configuration are much smaller than the experimental one[11], but in both configurations the Mach number is small, so is the Shear ($Sh = \delta_\nu / R$) number (tube large with respect to the boundary layer thickness) and the acoustic Reynolds number is high ($Re = \rho_0 c_0^2 / \mu_0 \omega$).

The simulations presented in this paper are performed with either isothermal straight wall boundary condition (wall with zero thickness) or a conducting straight wall with the isothermal boundary condition moved to the outer wall boundary. The geometry and thermo-physical characteristics of the surrounding wall (of the straight tube part) are discussed below.

An approximation of the axial streaming velocity $\overline{u}$ on the axis was obtained analytically[16] in the presence of a transverse temperature difference ΔT between the inner wall boundary and the guide axis, at low acoustic level and in a 2D geometry, under the hypotheses $\Delta T / T_0 \ll 1$ and $\delta_\nu / R \ll 1$. It was found[16] that $\overline{u}$ can be approximated as the Rayleigh solution with a first correction term introduced by Rott[24] depending on the Prandtl number, and a second correction term proportional to the product $\frac{\Delta T}{T_0}(\frac{R}{\delta_\nu})^2$, which becomes of order $O(1)$. A third correction term,

inversely proportional to $\hat{R} = \frac{R}{\delta_\nu}$, is negligible in the present applications. It follows that the streaming velocity on the axis can vanish or become negative for a large enough value of the transverse temperature difference ΔT, which is proportional to the inner longitudinal temperature difference between cold and hot regions. The latter is the result of thermoacoustic effect in the boundary layer and heat conduction through the wall. These results were combined to establish the following criterion on Re_{NL} for the streaming velocity to vanish on the axis[16]:

$$Re_{NL} \geq K_C \quad , \tag{2}$$

where

$$K_C = 30 \frac{k_s/k}{w/\delta_\nu} \left(1 + \frac{3}{2} \frac{1+Pr}{(\gamma-1)\sqrt{Pr}}\right) \frac{1}{(1-Pr^{3/2})}. \tag{3}$$

Although this result was obtained in the plane case, we expect it to provide a reasonable prediction in the axisymetric case. Note that K_C is a function of the wall thickness, of the thermophysical parameters for the wall and the gas, of the wave frequency, but not of the guide radius. In the relation given above for K_C, convection with the outside air is not taken into consideration. Two values of the radius of the straight tube are considered in the following, $R = 50\delta_\nu$ and $30\delta_\nu$ in order to assess the relevance of the criterion, Eq. (2).

In the numerical simulation, the thermophysical characteristics of the surrounding wall are chosen so that Eq. (2) could be satisfied for "physically" reasonable values of acoustic amplitudes. Specifically, the wall of the straight section is chosen to have a very small heat conduction coefficient. Indeed, taking a wall made of a standard material with thermal conductivity $k_s = 1.2$ W.m^{-1}.K^{-1} (e.g. pyrex, borosilicate-glass) would give $K_C = 3744$ from Eq. (3). For $\hat{R} = 30$, the corresponding Mach number would then have to be equal to 2 (and to 1.22 for $\hat{R} = 50$) in order to observe a nearly vanishing streaming flow along the axis, as seen in experiments. This is not suitable for the current context. Taking a very small value of k_s is a way around this problem. Therefore we consider a hypothetical material of thermal conductivity $k_s = 0.01$ W.m^{-1}.K^{-1}, density $\rho_s = 2230$ kg.m^{-3} and specific heat $c_s = 830$ J.kg^{-1}.K^{-1}. If the wall thickness is fixed at $w = 4\delta_\nu$, this gives $K_C = 31.2$. For $\hat{R} = 30$ the criterion will thus be satisfied for $U_{ac} \geq 64$ m.s^{-1} (and for $U_{ac} \geq 38.4$ m.s^{-1} in the case $\hat{R} = 50$). A third case will be considered for which the wall thickness is reduced to $w = \delta_\nu$, yielding a value for K_C multiplied by 4, $K_C = 124.8$. Therefore for $\hat{R} = 50$ the criterion will be satisfied for $U_{ac} \geq 76.8$ m.s^{-1}.

The grid is rectangular, uniform in the axial direction (x). The maximum radius of the domain (corresponding to the piston radius) is approximately $5R$ (Fig. 1). In the radial direction, the mesh is uniform for radius r less than R and stretched between R and $5R$ in the connecting tube. Following[8], there are 5 grid points per viscous boundary layer thickness, which has been shown to be the appropriate grid refinement. The corresponding mesh involves 750 points in the axial direction, and between 360 and 460 points in the radial direction. The time step is fixed according to the stability condition to $\delta t = 8 \times 10^{-9}$ s, corresponding to 6250 time iterations per period. When the heat equation is solved inside the non-zero thickness wall, the time necessary to reach steady-state is much longer than when the wall has zero thickness, since the thermal diffusion time scale across the wall ($\tau = w^2 \rho_s c_s / k_s$) is much larger than all other times scales. The value obtained is $\tau = 0.044$ s ($\simeq 884$ periods) for $w = \delta_\nu$ and $\tau = 0.7$ s ($\simeq 14000$ periods) for $w = 4\delta_\nu$. For the largest value of w, the simulations then require more than one hundred millions time steps to reach a nearly steady streaming flow.

III. NUMERICAL RESULTS. LOW ACOUSTIC LEVEL

The following results correspond to low acoustic level, with $U_{ac} = 2.92$ m.s^{-1} (piston displacement amplitude $0.3 \times 10^{-3} L$), $Re_{NL} = 0.18$. Results are presented for $\hat{R} = 50$ only, since the case $\hat{R} = 30$ is qualitatively similar.

In Fig. 2 is represented the velocity amplitude of the acoustic wave along the axis of the tube. Thanks to the anharmonic shape of the guide and to the low acoustic level, the oscillation is quasi-sinusoidal (the ratio of the amplitude of the second to the first harmonic at their respective antinode is 0.01). Figure 2 also shows that due to the guide geometry, the $x = 0$ position (that is the resonator mid-length) corresponds to an acoustic velocity node. At the

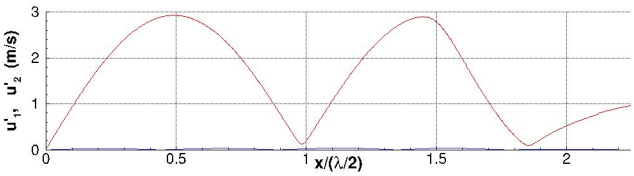

FIG. 2. Acoustic amplitude along the axis, $\hat{R} = 50, Re_{NL} = 0.18$: First harmonic (red), second harmonic (blue).

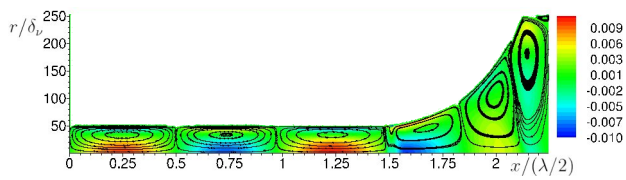

FIG. 3. Colored contours of axial streaming velocity (m.s^{-1}) with streamlines of the streaming flow on entire simulation domain, $\hat{R} = 50$, $Re_{NL} = 0.18$.

extremity of the guide, the boundary condition yields a non-zero acoustic velocity amplitude, associated with the moving piston that provides the necessary acoustic power, used to counteract the losses along the guide. These losses translate into the fact that the other minima of the acoustic velocity amplitude are not zeros, i.e. the nodes are pseudo-nodes or equivalently the wave is not purely standing. The same observation was made in the experiments [6,11].

Figure 3 shows the streamlines of the streaming flow superimposed to the contours of axial streaming velocity obtained in the entire simulation domain. There are 3 visible streaming cells in the straight part. As stated previously, the two streaming cells closest to the middle of the tube are not much affected by the converging section, and are analyzed thereafter.

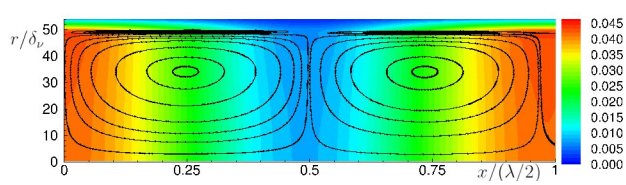

FIG. 4. Colored contours of the average temperature field (K) with streamlines of the streaming flow, $\hat{R} = 50$, $\hat{w} = 4$, $Re_{NL} = 0.18$.

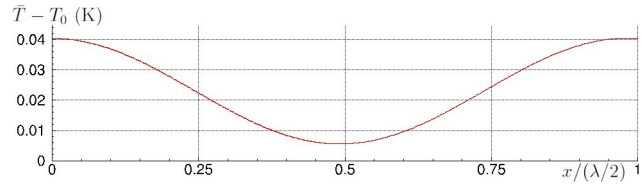

FIG. 5. Axial mean temperature $\overline{T} - T_0$ profile along the inner wall, $\hat{R} = 50$, $Re_{NL} = 0.18$.

Figure 4 shows the streamlines of the streaming flow and the mean temperature field $(\overline{T} - T_0)$ in the fluid domain $(0 \leq r/\delta_\nu \leq 50)$ and in the surrounding wall $(50 \leq r/\delta_\nu \leq 54)$ for $0 < x < \lambda/2$. The left cell has the theoretical length $\lambda/4$, while the right one is slightly shorter. The usual Rayleigh streaming flow is recovered, consistent with the distance between a velocity node and a pseudo-velocity node as seen in Fig. 2. The outer streaming velocity is of the same magnitude as that associated with the counter-rotating inner cell. As expected, the zone near the acoustic antinode becomes cooler than that near the nodes through thermoacoustic effect. Heat conduction within the fluid is then responsible for the steady temperature distribution given by Fig. 4. Figure 5 shows that the axial mean temperature $\overline{T} - T_0$ profile along the inner wall is sinusoidal, the maximum temperature difference between hot and cold fluid being $\Delta T = 0.035$K. Note that the coolest temperature is greater than T_0, meaning that there is global heating of the fluid. This could be due to viscous effects, and similar observations were made in[17]. In the wall the temperature distribution is linear in the transverse direction and sinusoidal in the axial direction, which is consistent with heat conduction in the wall with fixed outside temperature.

IV. NUMERICAL RESULTS. HIGH ACOUSTIC LEVEL

In this section, high acoustic level is considered (so-called "fast streaming" regime) in order to analyze the associated modification of the streaming flow. A first simulation is performed with a surrounding wall of zero-thickness (ideal isothermal boundary condition), illustrating the effect of reducing the harmonic content of the acoustic wave. Then the analysis is conducted accounting for a thick surrounding wall, with two

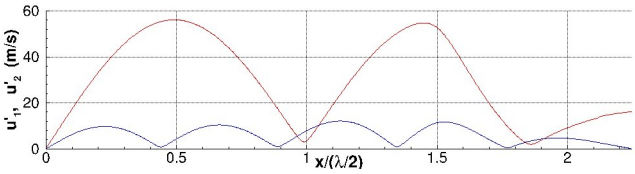

FIG. 6. Acoustic amplitude along the axis, $\hat{R} = 50$, $Re_{NL} = 55.4$, first harmonic (red), second harmonic (blue).

values of $\hat{R}$ and of $\hat{w} = w/\delta_\nu$ to assess the relevance of the criterion relation, Eq. (2).

A. Simulation with surrounding wall of zero-thickness (ideal isothermal boundary condition)

We first consider the effect of using the numerical configuration presented in Fig. 1 with a surrounding wall of zero-thickness, for $U_{ac} = 51.2$ m.s^{-1} (piston displacement amplitude $5 \times 10^{-3}L$), $Re_{NL} = 55.4$.

Figure 6 shows the velocity amplitude of the acoustic wave along the axis of the tube for $\hat{R} = 50$.

One can observe that the amplitude of the second harmonic of acoustic velocity at its antinode is approximately 20% of the amplitude of the first harmonic at its antinode. This is slightly larger than the amplitudes observed in experiments[4,6], which is to be expected considering that the acoustic velocity is larger in the numerical simulations than in the experiments. However this value remains compatible with the assumption of a monofrequency acoustic field: Assuming a superposition principle the magnitude of the streaming generated by this second-harmonic standing wave is expected to be only 4% of the magnitude of the streaming generated by the first harmonic, and is therefore negligible. In any case, there are no (or very weak) shock waves in this simulation.

Figure 7 shows the streamlines of the streaming flow superimposed to the contours of axial streaming velocity (top) and the temperature field (bottom) in a domain of axial extension $\lambda/2$. The outer streaming flow pattern is almost unchanged with respect to the low acoustic level case and no extra cell is generated. This can be explained by observing that temperature differences are small (a maximum value of 1.65 K). They are much smaller than in the simulations reported in[8] for a straight tube, where

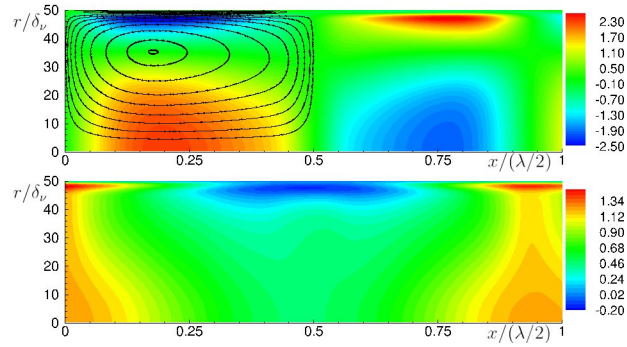

FIG. 7. Top: Colored contours of axial velocity (m.s^{-1}) with streamlines of streaming flow in the left part of the figure, $\hat{R} = 50$, $Re_{NL} = 55.4$ with surrounding wall of zero-thickness. Bottom: contours of relative mean temperature $\overline{T} - T_0$ (K).

shock waves were at the origin of large temperature differences (about 45 K for $Re_{NL} \approx 30$). Merkli and Thomann[17] have pointed out the effect of shock waves on the temperature field in an empty standing-wave guide. For this value of $\hat{R}$, the mean temperature difference is not large enough to significantly modify the streaming flow in the absence of shock waves. Therefore and despite the high value of the nonlinear Reynolds number, no extra streaming cell is generated. The case of a zero-thickness wall is indeed an ideal case with no physical application. The results obtained on this configuration show the necessity of including a conducting wall with non-zero thickness in order to reproduce the evolution of streaming patterns observed experimentally.

B. Simulations with conducting wall

In this section, the specific effect of taking into account the thickness and thermo-physical properties of the conducting wall is analyzed. The analysis is conducted in light of previous theoretical results summarized at the end of Section II B, pointing out temperature effects on acoustic streaming. Recall that the parameter given by Eq. (3) for this type of conducting wall and oscillating gas is $K_C = 31.2$ for $\hat{w} = 4$ and $K_C = 124.8$ for $\hat{w} = 1$. For $\hat{w} = 4$, we will present two cases ($\hat{R} = 30$ and $\hat{R} = 50$) with similar acoustic amplitudes and maximum mean temperature differences, but with different -although both large- values of Re_{NL}. For

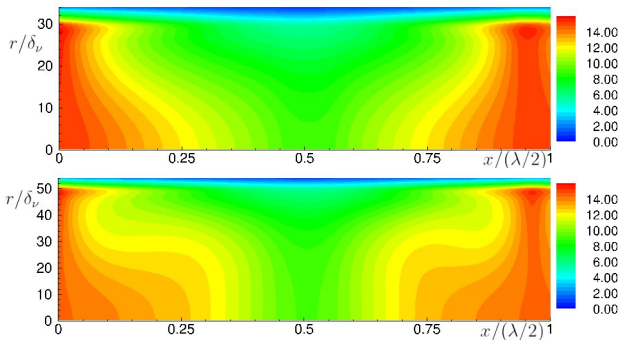

FIG. 8. Contours of the mean temperature field $\overline{T} - T_0$ (K) at steady state, time=25000 periods, with heat conduction solved in the wall, $\hat{w} = 4$. Top: $\hat{R} = 30$, $Re_{NL} = 24.6$, Bottom: $\hat{R} = 50$, $Re_{NL} = 66.5$.

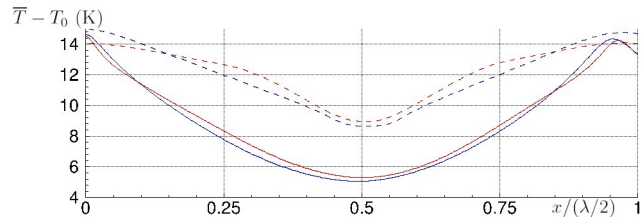

FIG. 9. Axial profile of the average temperature field $\overline{T} - T_0$ at steady state, $\hat{w} = 4$, along the axis (dashed) and the inner wall boundary (solid). Blue: $\hat{R} = 30$, $Re_{NL} = 24.6$; Red: $\hat{R} = 50$, $Re_{NL} = 66.5$.

$\hat{R} = 30$ the criterion of Eq. (2) is not satisfied and no extra streaming cell is expected. On the contrary, for $\hat{R} = 50$ the criterion is satisfied and an extra streaming cell is expected. Then, keeping the same value of Re_{NL} as in the last case we will show that if K_C is increased by decreasing the wall thickness ($\hat{w} = 1$) the criterion is not satisfied and no extra streaming cell develops.

The acoustic field is very similar to that presented for a wall with zero-thickness (Fig. 6), with no (or very weak) shock waves. As in Section IV A, the amplitude of the second harmonic of acoustic velocity at its antinode is approximately 20% of the amplitude of the first harmonic at its antinode (a little smaller in the case $\hat{R} = 30$). The acoustic amplitude of the first harmonic is equal to $U_{ac} = 56.8$ m.s^{-1} for $\hat{R} = 30$, yielding $Re_{NL} = 24.6 < K_C$. For $\hat{R} = 50$, in the case $\hat{w} = 4$ we obtain $U_{ac} = 56.1$ m.s^{-1} and $Re_{NL} = 66.5 > K_C$, and for $\hat{w} = 1$ the acoustic velocity is close with $U_{ac} = 58.6$ m.s^{-1}, yielding $Re_{NL} = 72.7 < K_C$.

For $\hat{w} = 4$, contours of the average temperature field can be compared for both values of $\hat{R}$ in Fig. 8, and longitudinal temperature profiles along the axis and the inside wall boundary are depicted in Fig. 9. As for the low acoustic level the left cell has the theoretical length $\lambda/4$, while the right one is slightly shorter, resulting in visible asymmetry of Fig. 8 and 9. These figures show that the temperature on the axis is several degrees hotter than on the wall, for both values of $\hat{R}$. The levels of temperature are the same (see color codes in Fig. 8), with a maximum temperature difference between cold and hot areas approximately equal to 10 K, but with a different spatial distribution due to different magnitudes of convective effects. In both cases, hot fluid is driven toward the acoustic velocity antinode near the axis $r = 0$, with stronger effect for $\hat{R} = 50$. Also, near the wall, cold fluid is driven toward the velocity node. This phenomenon results in a temperature field stratified in the radial direction in a large portion of the domain, with fluid hotter near the axis than near the wall (corresponding to the situation analyzed in[16]).

Although the temperature fields and levels are similar in the two cases, the effect on the modification of streaming patterns is much stronger for $\hat{R} = 50$. Figure 10 shows the streaming velocity field in a $\lambda/2$ area, for $\hat{R} = 30$ and $\hat{R} = 50$. Streamlines are superimposed to colored contours of the axial velocity. In both cases, the inner streaming flow pattern is almost unchanged (just slightly stretched towards the acoustic nodes). In the case $\hat{R} = 30$, the outer streaming flow patterns are not modified very much compared to the linear case. However one can see that the amplitude of the axial velocity on the axis is significantly lower than the amplitude in the inner streaming region (Fig. 10, top view). On the contrary, in the case $\hat{R} = 50$, the streaming flow pattern is very disturbed, resulting in a small reverse flow near the axis next to the acoustic antinode, which is consistent with experimental observations[4,6]. The maximum value of outer streaming axial velocity is even lower than for $\hat{R} = 30$ (Fig. 10, bottom view).

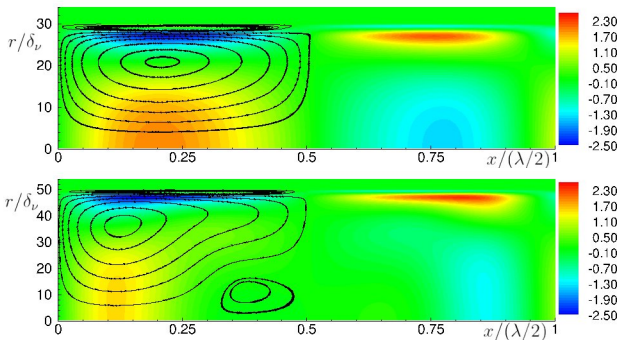

FIG. 10. Colored contours of axial velocity (m.s^{-1}) with streamlines of streaming flow represented in the left part of figures, $\hat{w} = 4$. Top: $\hat{R} = 30$, $Re_{NL} = 24.6$. Bottom: $\hat{R} = 50$, $Re_{NL} = 66.5$.

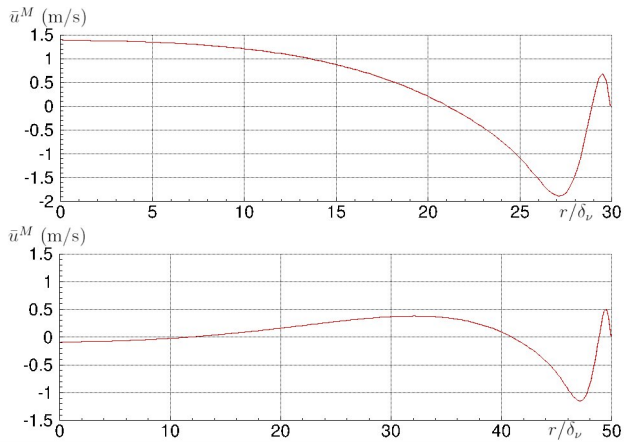

FIG. 11. Streaming axial velocity $\overline{u}^M$ along $x/(\lambda/2) = 0.4$, $\hat{w} = 4$. Top: $\hat{R} = 30$, $Re_{NL} = 24.6$. Bottom: $\hat{R} = 50$, $Re_{NL} = 66.5$.

The corresponding radial profiles of axial streaming velocity at $x/(\lambda/2) = 0.4$ (an axial position passing through the recirculation cell visible in Fig. 10) are shown in Fig. 11, for both values of $\hat{R}$. As expected, the inner streaming flow is unchanged in both cases. On the other hand, for $\hat{R} = 30$ the outer streaming velocity is parabolic with its maximum value on the axis, and for $\hat{R} = 50$ it decreases to become slightly negative on the axis.

If the wall thickness is chosen to be $\hat{w} = 1$, the value of K_C becomes $K_C = 124.8$. Running the calculation for $\hat{R} = 50$, $Re_{NL} = 72.7 < K_C$ shows that as expected, the outer streaming pattern, similar to that of Fig. 10 (top), is not distorted and no extra cell develops. These results show the relevance of the criterion given by Eq. (2) with the definition of parameter K_C given by Eq. (3) to assess the existence of an extra contra-rotating outer streaming cell in the region near the acoustic antinode. It shows the essential role of thermal effects in general and of heat conduction through the guide wall in particular.

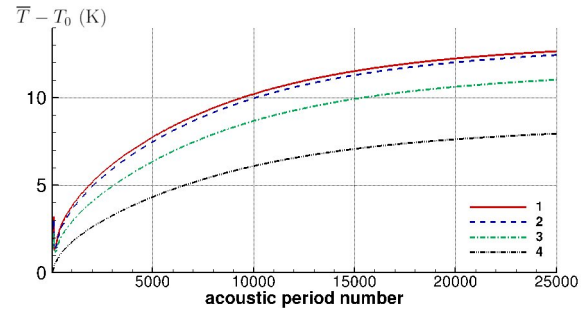

FIG. 12. Time evolution of the average temperature $\overline{T} - T_0$ at several radial positions, $\hat{R} = 50$, $Re_{NL} = 66.5$, $\hat{w} = 4$, $x/(\lambda/2) = 0.25$. 1=axis, 2=$\hat{R}/3$, 3=$2\hat{R}/3$, 4=$\hat{R}$.

C. Analysis of the time evolution of average temperature and streaming velocity.

In order to get more insight into the flow dynamics, the time evolutions of the streaming flow and mean temperature are analyzed for $\hat{R} = 50$, $\hat{w} = 4$ and $Re_{NL} = 66.5$. The temperature variation in time for several points located along the transverse section at $x = \lambda/8$ (in the middle of the streaming cell) for $\hat{R} = 50$ is reported in Figure 12: This figure shows that the radial temperature gradient is established soon after the wave is set in the guide, the temperature difference between fluid near the axis and near the wall being about 2 degrees after 1000 periods. The temperature difference between the axis and the wall is equal to 4.7 K at steady-state (Fig. 12). This is sufficient to create a reversed flow near the axis, since the criterion of Eq. (2) is satisfied.

Figure 13 shows the time evolution of the mean temperature at the acoustic velocity node, corresponding to the heated zone, on the axis ($r = 0$) and on the wall ($r = R$), for $\hat{R} = 50$. Conversely to Fig. 12, it appears that the time evolution of the temperature is homogeneous along the guide section. Comparing Fig. 12 and 13 thus permits to distinguish different stages in

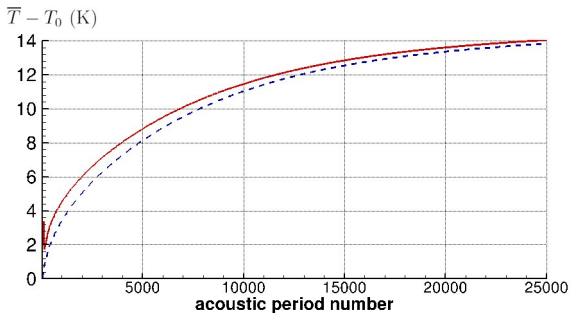

FIG. 13. Temperature evolution $\overline{T} - T_0$ at $x = 0$, $\hat{R} = 50$, $Re_{NL} = 66.5$, $\hat{w} = 4$. Solid red line: axis, Dashed blue line: $y = R$.

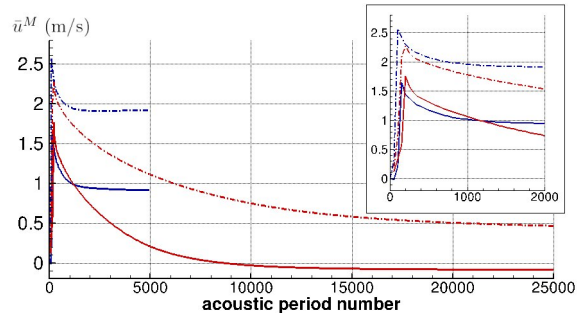

FIG. 14. Time evolution of the axial streaming velocity on the axis, $\hat{R} = 50$, $Re_{NL} = 66.5$, $\hat{w} = 4$, $x/(\lambda/2) = 0.25$ (red dash-dot) and $x/(\lambda/2) = 0.4$ (solid red). $Re_{NL} = 72.7$, $\hat{w} = 1$, $x/(\lambda/2) = 0.25$ (blue dash-dot) and $x/(\lambda/2) = 0.4$ (solid blue). Insert: zoom on first 2000 acoustic periods.

the transient evolution: Firstly thermoacoustic effect yields an increase of mean temperature in the whole velocity node region; then streaming flow convects heat from the velocity node region towards the velocity antinode near the axis.

The time evolution of the axial streaming velocity for two different locations along the axis is shown in Figure 14, for $\hat{R} = 50$ and $Re_{NL} \simeq 70$, for two values of the wall thickness, $\hat{w} = 4$ (in which case $Re_{NL} > K_C$) and $\hat{w} = 1$ (for which $Re_{NL} < K_C$). For $\hat{w} = 4$ it can be observed that the velocity follows a time evolution correlated with the mean temperature evolution (Fig. 12 and 13): It decreases with time and stabilizes over a long time that corresponds to the establishment of a transverse mean temperature gradient (about 15000 periods). At position $x/(\lambda/2) = 0.4$, the sign of the axial velocity changes after about 10000 acoustic periods, which indicates the appearance of a reversed cell.

For $\hat{w} = 1$, $Re_{NL} = 72.7 < K_C$ and the axial streaming velocity remains positive at both locations, which is to be expected since there is no extra cell. In accordance with the estimate of the characteristic heat conduction time across the wall, steady state is established much faster than in the case $\hat{w} = 4$.

It is also interesting to analyze the evolution of the temperature field, especially during the appearance of the extra cell. Let us first recall that as shown by Fig. 4, at low acoustic level, the average temperature is stratified horizontally: in a given transverse section the temperature is mostly uniform, satisfying the symmetry condition on the axis, $\frac{\partial \overline{T}}{\partial r} = 0$. These features change at high acoustic level due to convection by the streaming flow that becomes important. The top figure of Fig. 15 shows the radial profile of average temperature for $x/(\lambda/2) = 0.4$ ($\hat{R} = 50$, $Re_{NL} = 66.5$, $\hat{w} = 4$), 2500 periods after the acoustic wave is set in the guide. It shows that the averaged temperature fits a quadratic curve in r for the first half of the section (which is also compatible with the symmetry condition on the axis). This reveals the appearance of a radial temperature gradient. This gradient then causes the decrease of the streaming flow, according to the analysis developed in[16] and summarized at the end of Section II B. The decrease of the streaming velocity towards zero in turn induces a decrease of the radial temperature gradient. This is illustrated by the bottom figure of Fig. 15 that shows the radial profile of average temperature for $x/(\lambda/2) = 0.4$, in the established regime (25000 periods) together with a constant fit.

This process converges towards vanishing radial temperature gradient as well as streaming velocity. Thus the additional streaming cell that characterizes high acoustic levels turns into a zone of almost stagnant streaming flow. This corresponds to the axial streaming velocity on the axis at $x/(\lambda/2) = 0.4$ remaining around zero once it has vanished (see Fig. 14).

When the acoustic amplitude is further increased, the same structure of the streaming flow can be observed and a large stagnant flow area is still present near the acoustic velocity antinode. The overall outer streaming flow amplitude decreases in a stabilization -or saturation- manner.

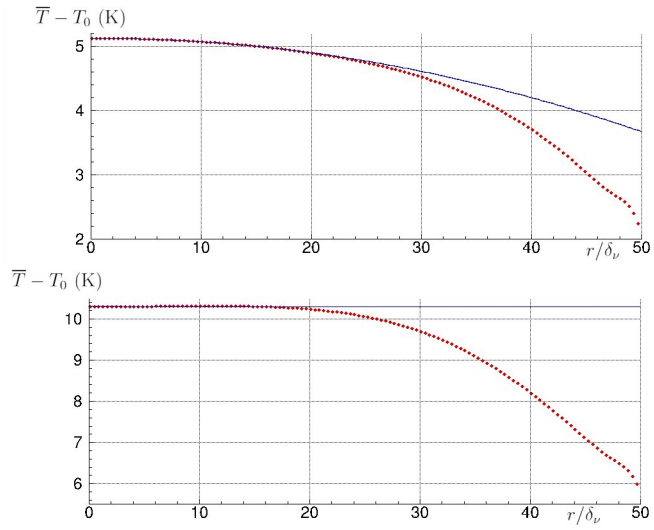

FIG. 15. Average temperature (red dots) along r/δ_ν, $x/(\lambda/2) = 0.4, \hat{R} = 50, Re_{NL} = 66.5, \hat{w} = 4$. Top: time=2500 periods, with quadratic fit on first 100 points (blue line). Bottom: Time=25000 periods, with constant fit on first 90 points (blue line).

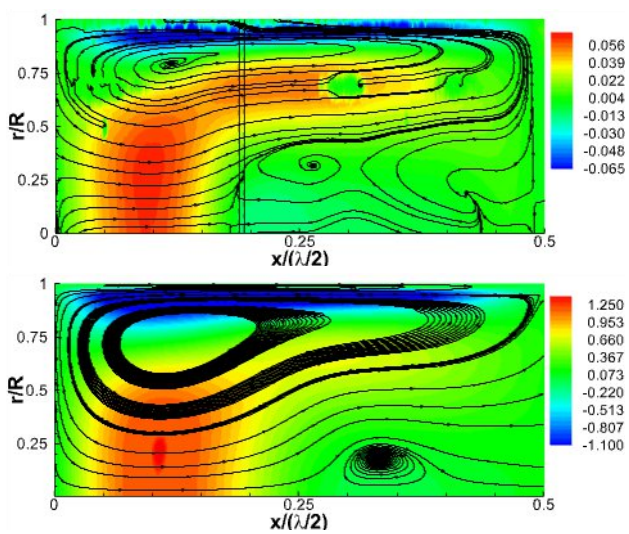

FIG. 16. Streamlines of Eulerian streaming flow colored by contours of axial Eulerian streaming velocity (m.s^{-1}). Top: Experimental result[6], $\hat{R} = 140$, $K_C = 11$, $Re_{NL} = 30$. Bottom: Numerical result, $\hat{R} = 50$, $K_C = 31.2$, $Re_{NL} = 66.5$.

Figure 16 illustrates the comparison in a $\lambda/4$ area of the Eulerian streaming velocity field obtained from experiments[6], and the present numerical simulations. The visual agreement is remarkable and the stagnant zone near the acoustic velocity antinode is clear in both images. This comparison validates the $Re_{NL} > K_C$ criterion: Even though geometrical and physical parameters are quite different, the criterion $Re_{NL} > K_C$ is satisfied in both cases and the streaming flow dynamics is qualitatively the same.

V. CONCLUSION

The coupling between thermal effects and outer Rayleigh streaming in standing wave guides was analyzed numerically. An axisymmetric numerical configuration was introduced to investigate the evolution of the streaming flow structure and average temperature field at increasing acoustic levels. The numerical domain mimicked the experimental setup used in[6] to avoid the development of shock waves, which was a novelty of this study. The simulations highlighted the crucial role of heat conduction in the wall and the effect of a transverse average temperature difference on the structure of outer streaming cells. We had shown in a recent paper that a reverse streaming cell could form if the classical nonlinear Reynolds number exceeded a value K_C depending on the wave frequency and on thermophysical properties of the fluid and solid wall. Indeed, as the acoustic level was increased, the average temperature field became stratified transversely, and the maximum outer streaming velocity decreased. Simulations showed the relevance of the criterion for predicting the appearance of new contra-rotating outer streaming cells of small velocity amplitude near the acoustic velocity antinodes.

For higher acoustic levels these new cells evolved into large stagnant zones where the streaming flow was of very small amplitude and the temperature field radial stratification decreased. The overall outer streaming flow decreased in a stabilization -or saturation- manner. The present simulations correctly reproduced experimental findings.

This study concludes our search of the physical mechanisms responsible for the complex evolution of outer streaming patterns observed from low to high acoustic levels[9,11]. Our isentropic simulations showed that non linear coupling between acoustic and streaming flows is a necessary mechanism to explain the appearance of the extra streaming cell under isentropic conditions (inertial effects alone cannot explain the evolution of the streaming flow)[9,12]. Our present

simulations of the fully compressible Navier-Stokes equations show that the intricate non-linear coupling between acoustic streaming and heat transfer is the most important mechanism, highlighting the crucial role of thermally controlled boundaries. Non linear coupling between acoustic and streaming flows still holds but is much weaker than that between acoustic streaming and heat transfer.

These findings will be useful to further investigate streaming in practical applications; among those, it is still necessary to clarify the balance between thermoacoustic effect, natural convection, end effects and acoustic streaming in real thermoacoustic devices.

ACKNOWLEDGMENTS

Virginie Daru wants to thank Nicolas Alferez for his help in parallelizing the computer code and for letting her use his computer for some of the present simulations.

[1] L. Rayleigh, "On the circulation of air observed in Kundt's tubes, and on some allied acoustical problems", Philos. Trans. R. Soc. London **175**, 1–21 (1884).

[2] J. R. Olson and G. W. Swift "Acoustic streaming in pulse tube refrigerators: Tapered pulse tubes", Cryogenics. **37**, 769–776 (1997).

[3] J. Lighthill "Acoustic streaming.", J. Sound. Vib. **61**, 391–418 (1978).

[4] M. Thompson, A. Atchley and M. J. Maccarone, "Influences of a temperature gradient and fluid inertia on acoustic streaming in a standing wave.", J. Acoust. Soc. Am. **117(4)**, 1839–1849 (2004).

[5] S. Moreau, H. Bailliet, and J.-C. Valière, "Measurements of inner and outer streaming vortices in a standing waveguide using laser Doppler velocimetry", J. Acoust. Soc. Am. **123**, 640–647 (2008).

[6] I. Reyt, H. Bailliet, and J.-C. Valière, "Experimental investigation of acoustic streaming in a cylindrical waveguide up to high streaming Reynolds numbers", J. Acoust. Soc. Am. **135**, 27–37 (2014).

[7] S. Boluriaan and P. J. Morris, "Numerical simulation of acoustic streaming in high amplitude standing wave", 9th AIAA/CEAS Aeroacoustics Conference and Exhibit 12-14 May 2003, Hilton Head, SC, AAIA paper 2003-3152 (12-14 mai 2003).

[8] V. Daru, D. Baltean-Carlès, C. Weisman, P. Debesse and G. Gandikota, "Two-dimensional numerical simulations of nonlinear acoustic streaming in standing waves.", Wave Motion **50**, 955–96 (2013).

[9] V. Daru, I. Reyt, H. Bailliet, C. Weisman and D. Baltean-Carlès, "Acoustic and streaming velocity components in a resonant wave guide at high acoustic levels.", J. Acoust. Soc. Am. **141(1)**, 563–574 (2017).

[10] L. Menguy and J. Gilbert, "Non-linear acoustic streaming accompanying a plane stationary wave in a guide", Acta Acustica **86**, 249–259 (2000).

[11] I. Reyt, V. Daru, H. Bailliet, S. Moreau, J.-C. Valière, D. Baltean-Carlès, and C. Weisman, "Fast acoustic streaming in standing waves: Generation of an additional outer streaming cell", J. Acoust. Soc. Am. **134**, 1791–1801 (2013).

[12] V. Daru, C. Weisman, D. Baltean-Carlès, I. Reyt and H. Bailliet, "Inertial effects on acoustic Rayleigh streaming flow: Transient and established regimes.", Wave Motion **74**, 1–17 (2017).

[13] M. Cervenka and M. Bednarik, "Effect of inhomogeneous temperature fields on acoustic streaming structures in resonators.", J. Acoust. Soc. Am. **141**, 4418–4426 (2017).

[14] M. Cervenka and M. Bednarik, "Numerical study of the influence of the convective heat transport on acoustic streaming in a standing wave.", J. Acoust. Soc. Am. **143(2)**, 727–734 (2018).

[15] G. Michel and G. P. Chini, "Strong wave-mean-flow coupling in baroclinic acoustic streaming.", J. Fluid Mech. **858**, 536–564 (2019).

[16] V. Daru, C. Weisman, D. Baltean-Carlès and H. Bailliet, "Acoustically induced thermal effects on Rayleigh streaming.", J. Fluid Mech. **911, A7**, 1–22 (2021).

[17] P. Merkli and H. Thomann, "Thermoacoustic effects in a resonance tube.", J. Fluid Mech. **70**, 161–177 (1975).

[18] A. Alexeev and C. Gutfinger, "Resonance gas oscillations in closed tubes: Numerical study and experiments.", Physics of Fluids **15 (11)**, 3397-3408 (2003).

[19] Y. Lin and B. Farouk, "Heat transfer in a rectangular chamber with differentially heated horizontal walls: Effects of a vibrating sidewall.", Int. J. Heat Mass Transfer **51**, 3179–3189 (2008).

[20] A. A. Gubaidullin and A. V. Yakovenko, "Effects of heat exchange and nonlinearity on acoustic streaming in a vibrating cylindrical cavity.", J. Acoust. Soc. Am. **137**, 3281-3287 (2015).

[21] P. De Palma, M. D. De Tullio, G. Pascazio and M. Napolitano, "An immersed-boundary method for compressible viscous flows.", Computers & Fluids **35**, 693–702 (2006).

[22] C. W. Hirt, A. A. Amsden and J. L. Cook, "An arbitrary Lagrangian-Eulerian computing method for all flow speeds.", J. Comp. Phys. **14**, 227–253 (1974).

[23] V. Daru and C. Tenaud, "High order one-step monotonicity preserving schemes for unsteady flow calculations.", J. Comp. Phys. **193**, 563–594 (2004).

[24] N. Rott, "The influence of heat conduction on acoustic streaming.", Zeitschrift für Angewandte Mathematik und Physik (ZAMP) **25**, 417–421 (1974).